Interpretable principal component analysis for multilevel multivariate functional data

JUN ZHANG

Department of Biostatistics, University of Pittsburgh, 130 De Soto Street, Pittsburgh, PA, 15261, USA

GREG J. SIEGLE [iD]

Department of Psychiatry, University of Pittsburgh, 3811 O'Hara Street, Pittsburgh, PA, 15213, USA

TAO SUN

Center for Applied Statistics, School of Statistics, Renmin University of China, 59 Zhongguancun Street, Beijing, 100872, China

WENDY D'ANDREA

Department of Psychology, New School for Social Research, 80 Fifth Avenue, New York, NY, 10011, USA

ROBERT T. KRAFTY [iD] *

Department of Biostatistics and Bioinformatics, Emory University, 1518 Clifton Road NE, Atlanta, GA, 30322, USA

rkrafty@emory.edu

SUMMARY

Many studies collect functional data from multiple subjects that have both multilevel and multivariate structures. An example of such data comes from popular neuroscience experiments where participants' brain activity is recorded using modalities such as electroencephalography and summarized as power within multiple time-varying frequency bands within multiple electrodes, or brain regions. Summarizing the joint variation across multiple frequency bands for both whole-brain variability between subjects, as well as location–variation within subjects, can help to explain neural reactions to stimuli. This article introduces a novel approach to conducting interpretable principal components analysis on multilevel multivariate functional data that decomposes total variation into subject-level and replicate-within-subject-level (i.e., electrode-level) variation and provides interpretable components that can be both sparse among variates (e.g., frequency bands) and have localized support over time within each frequency band. Smoothness is achieved through a roughness penalty, while sparsity and localization of components are achieved by solving an innovative rank-one based convex optimization problem with block Frobenius and matrix L_1-norm-based penalties. The method is used to analyze data from a study to better understand reactions to emotional information in individuals with histories of trauma and the symptom of dissociation, revealing

*To whom correspondence should be addressed.

new neurophysiological insights into how subject- and electrode-level brain activity are associated with these phenomena. Supplementary materials for this article are available online.

Keywords: Convex optimization; Functional principal component analysis; Multilevel models; Psychological trauma; Regularization.

1. INTRODUCTION

Functional principal components analysis (FPCA) is arguably one of the most popular tools for analyzing functional data, providing low-dimensional, parsimonious measures that account for the majority of variation. There has been growing interest in FPCA for multiple dependent functional processes, such as when multiple curves are observed for each subject. Depending on the characteristics of the data and the scientific questions of interest, multiple functional processes are typically analyzed either through multivariate FPCA, aiming to describe joint variation of different processes (Rice and Silverman, 1991; Ramsay and Silverman, 2005; Chiou *and others*, 2014; Happ and Greven, 2018) or through multilevel FPCA, aiming to characterize variation from repeatedly observed curves with a multilevel hierarchical structure (e.g., between- and within-subject level principal components) (Crainiceanu *and others*, 2009; Di *and others*, 2009; Greven *and others*, 2010; Staicu *and others*, 2010; Zipunnikov *and others*, 2011; Shou *and others*, 2015; Goldsmith *and others*, 2015; Scheffler *and others*, 2019).

An increasing number of studies collect and wish to analyze functional data that can be viewed simultaneously as multilevel and multivariate. A popular example is from electroencephalography (EEG), which measures electrical activities that take the form of multiple curves over time, defined over multiple pre-specified frequency bands, and recorded from multiple locations across the scalp Our motivating example, which is described in further detail in Section 2, involves the analysis of such data from a study to better understand biological mechanisms of feelings of numbness and being removed from reality. To illustrate these data, Figure 1 displays data from two of four time-varying frequency-band measurements of brain activity, at 2 of 14 measured locations across the scalp. Such data can be considered multivariate across frequency-band measures, where we desire a summary of the joint information across the multiple frequency bands, as well as multilevel across locations, where we consider both whole-brain variability between participants as well as location-variation within participants.

Although methods for multivariate FPCA and for multilevel FPCA have been individually extensively studied, and methods for FPCA of other data structures such as longitudinally observed functional data (Chen and Müller, 2012; Hasenstab *and others*, 2017; Scheffler *and others*, 2019) have also been studied, there is a dearth of methods that are able to jointly deal with both multivariate and repeatedly measured functional processes. A contribution of this article is the introduction of a method for FPCA of multilevel multivariate functional data. Specifically, we extend the multilevel decompositions in Di *and others* (2009) and Shou *and others* (2015) to multivariate processes through latent random multivariate subject-specific processes and replicate-within-subject processes and assume a separable replicate-temporal covariance structure that can account for correlation among data from the same subject, such as spatial correlation among data from different locations across the scalp.

The major contribution of this article is the development of an interpretable approach to the PCA of multiple functional processes that is not only smooth but also localized within time and among the variates. Existing approaches to conducting FPCA on multivariate functional data are limited in that they are not localized, or that each component is a nontrivial function of each variate at all time points. This lack of localization, which is a common issue across most classical procedures for analyzing functional data, can be problematic in that it obstructs interpretation. The benefit of localized procedures, both for providing scientifically interpretable measures and for improving statistical performance, have been previously discussed in the context of functional linear regression (James *and others*, 2009;
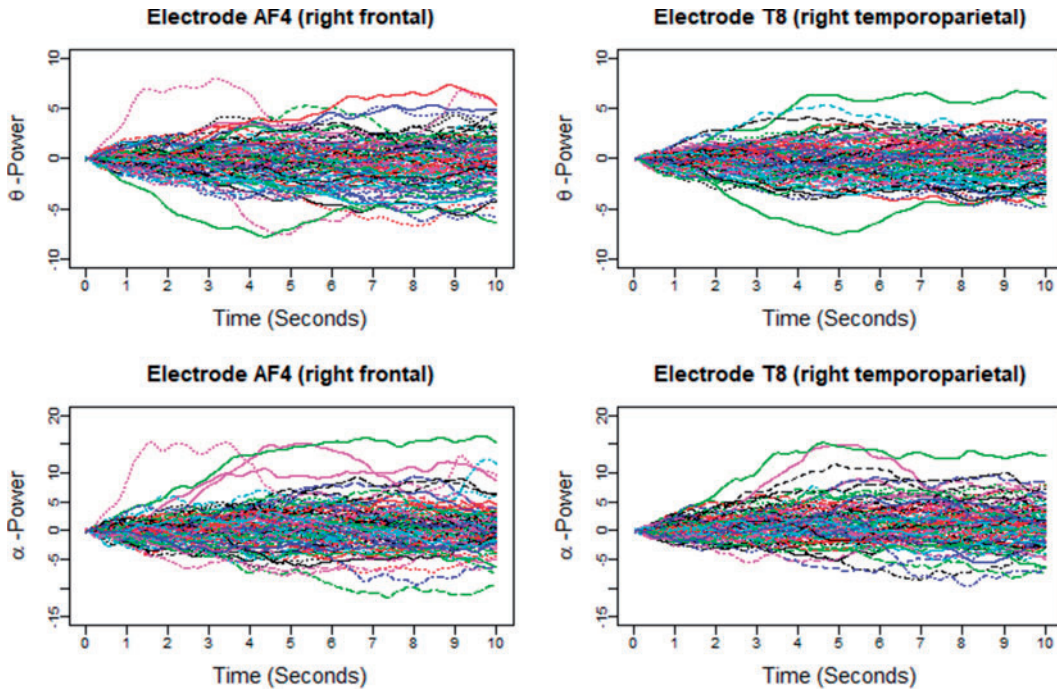
Fig. 1. Illustration of the Blunted and Discordant Affect (BADA) study data: time-varying power in two (theta and alpha power) of four considered bands at two (AF4, right frontal and T8, right temporoparietal) locations.

Zhao *and others*, 2012; Zhou *and others*, 2013) and in the context of univariate FPCA (Chen and Lei, 2015; Lin *and others*, 2016). However, to the best of our knowledge, localization for the PCA of multivariate functional data has yet to be addressed. The problem of conducting an interpretable FPCA for multivariate processes is considerably more challenging than for univariate, as it needs to allow for localization not only within time, but also for localization among the variates.

Towards the goal of conducting an interpretable multivariate FPCA, we introduce a novel localized sparse-variate FPCA (LVPCA). The LVPCA incorporates a roughness penalty to assure smoothness, and matrix L_1 and block-wise Frobenius norm-based penalties to achieve localization within time and variate, respectively. The use of this combination of penalties can be viewed as a multivariate FPCA analogue of the vector L_1 and block-wise vector L_2 norms that are used to achieve within- and between-group sparsity in high-dimensional regression by the sparse-group Lasso (Simon *and others*, 2013). There are two main challenges when incorporating localization or sparsity into a PCA: direct approaches via rank-one projection matrices provide solutions that, if they exist, are NP-hard and they provide components that are not orthogonal. The LVPCA overcomes the first issue through the use of the Fantope, which is the convex hull of rank-one projection matrices and has been adapted to overcome analogous problems in localized univariate FPCA (Chen and Lei, 2015) and sparse high-dimensional PCA (Vu *and others*, 2013). The separation of the smoothness penalty and the localization and sparsity penalties enables the problem to be embedded into the Fantope and allows the LVPCA to be formulated as a convex optimization problem. The second issue is overcome through Fantope-deflation, which assures orthogonality of successive components. The formulation as a convex optimization problem allows for the development of an alternating direction method of multipliers (ADMM) algorithm (Boyd *and others*, 2011) for easy implementation. For multilevel multivariate FPCA, LVPCA is applied to the MoM estimators of the subject-specific and replicate-within-subject covariance operators to provide interpretable FPCA at each level.

The rest of the article is organized as follows. The motivating BADA Study is introduced in Section 2. A principal components model for multilevel multivariate functional data is presented in Section 3 and an accompanying estimating procedure is developed in Section 4. The proposed method is used to analyze simulated data in Section 5 and data from the motivating BADA Study in Section 6. Finally, we discuss and conclude in Section 7.

2. MOTIVATING STUDY

Data were examined from the Blunted and Discordant Affect (BADA) study, which was conducted to better understand individual differences in emotional information processing. Multiple psychopathologies such as depression and post-traumatic stress disorder (PTSD) are characterized by intense repetitive negative self-thoughts (rumination), which is increasingly well understood. These same conditions are also characterized by blunted emotional reactions and feelings of distance from the self and reality (dissociation) in response to negative information, particularly in the presence of chronic trauma or abuse backgrounds. The neural basis of such blunted reactions are less well understood. As treatments for depression and PTSD are commonly devoted to reducing negative emotion, if some individuals are already neurally disengaged or blunted in their responses, this traditional approach may not be beneficial. Thus, the BADA study examined individuals selected for a variety of psychopathologies, including those with and without chronic trauma, on tasks that could yield with blunted reactions in vulnerable individuals.

We consider data from $N = 106$ study participants whose brain activity was recorded via EEG while ruminating on a negative thought for 10 s. The EEG montage included 14 electrodes placed in selected locations on the scalp (Figure 4(A)). Data were recorded at 128 Hz. Frequency-band measures, or the amount of variability within an EEG time series due to osculations within an interval of frequencies, provide interpretable measures that are used by researchers and clinicians to elucidate neurophysiological mechanisms. Frequency-band measures are not independent and rather, often have high correlation. We consider four measures: theta power (4–7 Hz) linked to memory and emotional regulation (Knyazev, 2007), alpha power (8–12 Hz) that reflects relaxation, disengagement, or a lack of cognitive activity (Davidson *and others*, 1990), beta power (18–25 Hz) linked to a variety of attentional processes (Neuper *and others*, 2009), and gamma power (39–45 Hz) associated with feature integration and fundamental cognitive processes (Tallon-Baudry and Bertrand, 1999). Additional technical details with regards to data processing are provided in Supplementary material available at *Biostatistics* online.

We desire an analysis of these data to address three questions. First, we desire low-dimensional measures that can be used to describe variability in neurophysiological reactivity in participants while ruminating on negative thoughts. We are specifically interested in neurally meaningful phenomena that could vary anywhere throughout the brain (i.e., have different topographies across participants) and across participants, but have unique time and frequency-band characteristics. Second, we desire an understanding of the association between these measures with clinical measures of dissociation, measured through the square-root transformed score on the Dissociative Experiences Scale (DES) (Bernstein and Putnam, 1986), in order to better understand neurophysiological mechanisms behind blunted reactions and lack of normal integration of thoughts, feelings and experiences into the stream of consciousness and memory. Lastly, blunted affect has been observed in individuals with a history of trauma and the mechanism driving blunted affect could be different among those with and without a history of trauma (Miniati *and others*, 2010). We are interested in understanding the potential role that trauma plays in moderating the relationship between dissociation and neurophysiology.

3. MODEL

The primary methodological question considered in this article is how to conduct interpretable principal component analyses that summarize the variability of multilevel multivariate functional data, $Y_{ij}(t) =$

$\{Y_{ij}^{(1)}(t), ..., Y_{ij}^{(M)}(t)\}$, observed from $i = 1, ..., N$ subjects, with $j = 1, ..., J$ repeated measures taken for each subject at M variates. In the motivating study, there are $N = 106$ participants, $J = 14$ electrodes and $M = 4$ frequency band measures. We consider the scenario where curves for each variate from each subject are observed over a common dense grid of P time points as is typical for EEG data, $t_1 < ... < t_P \in \mathcal{T}$, and where the design is balanced with an equal number of repeated measures J for each subject. Discussions with regards to the unbalanced design and to the setting where curves are observed either sparsely or over different time points are given in Section 7.

Consider a two-way functional ANOVA model

$$Y_{ij}(t) = \mu(t) + \eta_j(t) + Z_i(t) + W_{ij}(t) + \epsilon_{ij}(t), \tag{3.1}$$

where $\mu(t)$ and $\eta_j(t)$ are fixed effects. In our motivating example, they represent the overall mean function and electrode-specific shifts from the overall mean function. The random process $Z_i(t)$ is the zero-mean subject-level deviation from the electrode-specific mean function, with a between-subject covariance function $K_z(t, s) = \mathrm{E}[Z_i(t)Z_i(s)^T]$. The random process $W_{ij}(t)$ is the zero-mean correlated electrode-level deviation from the subject-level mean, with a within-subject covariance function $K_w(t, s) = \mathrm{E}[W_{ij}(t)W_{ij}(s)^T]$. The processes $W_{ij}(t)$ and $Z_i(t)$ are assumed to be uncorrelated, and $\epsilon_{ij}(t)$ is white noise with mean 0 and variance σ^2.

Within each subject, we assume that the covariance between $W_{ij}(t)$ and $W_{ik}(s)$ at electrode j and k is separable, and takes the form

$$\mathrm{E}\left[W_{ij}(t)W_{ik}(s)^T\right] = \rho_{jk}K_w(t, s),$$

where ρ_{jk} is the correlation coefficient between electrode-level deviations. Another interpretation for ρ_{jk} is the correlation between observations at electrode j and k beyond the dependency accounted by the subject-level random process. We assume that ρ_{jk} is sparse such that ρ_{jk} is nonzero for only a subset of pairs of electrodes. Two things should be noted. First, sparsity in ρ_{ij} assures identifiability. If no structure was assumed on the correlation between W_{ij} and W_{ik}, then it would be unidentifiable with K_z. Second, this assumption is different than the assumption made in other multilevel principal component models where within-subject correlation is modeled as a vanishing stationary function of known structural distance (Staicu *and others*, 2010). In the analysis of EEG, data from different electrodes from the same subject are expected to be correlated not only due to the structural spatial location of the electrodes but also due to functional relationships and networks. Although the spatial distance between different electrodes are known, functional relationships are not. Thus, we make the nonparametric assumption that ρ_{jk} is sparse.

When the processes $Z_i(t)$ and $W_{ij}(t)$ are square-integrable, the Karhunen–Loeve expansion allows the model in 3.1 to be expressed as

$$Y_{ij}(t) = \mu(t) + \eta_j(t) + \sum_{r=1}^{\infty} \xi_{ir}^z \phi_r^z(t) + \sum_{r=1}^{\infty} \xi_{ijr}^w \phi_r^w(t) + \epsilon_{ij}(t), \tag{3.2}$$

where $\phi_r^z(t)$ and $\phi_r^w(t)$ are the rth eigenfunctions of $K_z(t, s)$ and $K_w(t, s)$, respectfully. The principal component scores $\xi_{ir}^z = \int_{t \in \mathcal{T}} Z_i^T(t)\phi_r^z(t)dt$ and $\xi_{ijr}^w = \int_{t \in \mathcal{T}} W_{ij}^T(t)\phi_r^w(t)dt$ are mean-zero random variables with $\mathrm{var}(\xi_{ir}^z) = \theta_r^z$, $\mathrm{var}(\xi_{ijr}^w) = \theta_r^w$, $\mathrm{cov}(\xi_{ijr}^w, \xi_{ikr}^w) = \rho_{jk}\theta_r^w$ and are uncorrelated otherwise.

The goal of our analysis is to conduct a FPCA by obtaining interpretable estimates of the level-specific weight functions ϕ_r^z and ϕ_r^w, which provide a low-dimensional representation of the major modes of variation, and of the level-specific principal component scores ξ_{ir}^z and ξ_{ijr}^w. This FPCA is multivariate in that the weight functions are M-dimensional and it is multilevel in that it provides subject-level

components to describe subject-average variability and electrode-within-subject-level scores to describe within-subject variation.

4. ESTIMATION

In this section, we develop a two-stage estimation procedure for conducting interpretable multilevel multivariate FPCA. The first stage discussed in Section 4.1 obtains MoM estimators of the between- and within-subject covariances, $K_z(t, s)$ and $K_w(t, s)$. The second stage discussed in Section 4.2 utilizes a novel penalized decomposition of the level-specific MoM estimator, which we refer to as localized sparse-variate functional principal component analysis (LVPCA), that produces interpretable components and weight functions that are smooth as functions of time, sparse among variates, and localized in time within variates. An optimization algorithm for computing LVPCA is offered in Section 4.3.

4.1. *Covariance matrix estimation*

To aid computation, we introduce additional notation and vectorize values of the mth variate from electrode j from subject i as $Y_{ij}^{(m)} = \{Y_{ij}^{(m)}(t_1), ..., Y_{ij}^{(m)}(t_P)\}^T$, then concatenate these M vectors to formulate a $PM \times 1$ vector $Y_{ij} = \{Y_{ij}^{(1)T}, ..., Y_{ij}^{(M)T}\}^T$, $i = 1, ..., N, j = 1, ..., J$. The $MP \times MP$ matrices K_z and K_w are defined using the same concatenation such that the $[(m-1)P + p], [(\ell - 1)P + q]$ elements of K_z and K_w are the (m, ℓ) elements of $K_z(t_p, t_q)$ and $K_w(t_p, t_q)$, respectively. Similarly, we vectorize values of the rth eigenfunction within the mth variate $\phi_r^{(m)} = \{\phi_r^{(m)}(t_1), ..., \phi_r^{(m)}(t_P)\}^T$, then concatenate these M vectors to obtain the rth eigenvector $\phi_r = \{\phi_r^{(1)T}, ..., \phi_r^{(M)T}\}^T$. Lastly, we let the $MP \times NJ$ matrix $Y = \{Y_{11}, ..., Y_{1J}, ..., Y_{N1}, ..., Y_{NJ}\}$.

Without loss of generality, we assume that $Y_{ij}(t)$ has been demeaned by subtracting the electrode-specific mean, so that $\mu(t) + \eta_j(t) = 0$, in order to focus on the estimation of K_z and K_w. We begin by noting that

$$E\{Y_{ij}(t) Y_{ij}(s)^T\} = K_w(t, s) + K_z(t, s) + \sigma^2 I(t = s)I$$

$$E\{Y_{ij}(t) - Y_{ik}(t)\}\{Y_{ij}(s) - Y_{ik}(s)\}^T = 2\left[K_w(t, s)(1 - \rho_{jk}) + \sigma^2 I(t = s)I\right], \quad j \neq k.$$

The estimation procedure depends on an initial unbiased estimator of the within-subject correlation $\hat{\rho}_{jk}$. Details with regards to the estimation of $\hat{\rho}_{jk}$ are provided in Supplementary material available at *Biostatistics* online. Define the matrices $F_z = K_w + K_z + \sigma^2 I$ and $F_w = cK_w + \sigma^2 I$, where $c = \frac{J - \frac{1}{J}\sum_{j=1}^{J}\sum_{k=1}^{J}\hat{\rho}_{jk}}{J - 1}$. The explicit MoM estimators of F_z and F_w are given by

$$\widehat{F}_z = \frac{1}{NJ}\sum_{i=1}^{N}\sum_{j=1}^{J} Y_{ij}Y_{ij}^T$$

$$\widehat{F}_w = \frac{1}{2NJ(J-1)}\sum_{i=1}^{N}\sum_{j=1}^{J}\sum_{k \neq j}(Y_{ij} - Y_{ik})(Y_{ij} - Y_{ik})^T.$$

The covariance estimators can then be obtained as $\widehat{K}_z = \widehat{F}_z - \frac{1}{c}\widehat{F}_w$, $\quad \widehat{K}_w = \frac{1}{c}\widehat{F}_w$.

If there is no measurement error, $\widehat{K}_z$ and $\widehat{K}_w$ are consistent estimators of K_z and K_w. In the presence of noise, as in our case, the off-diagonal terms are consistent estimators, but there exists a nugget effect on the diagonal. This nugget effect will be explicitly accounted for through a smoothing penalty when estimating eigenvectors.

4.2. *LVPCA: localized sparse-variate functional principal component analysis*

In the second stage, we obtain interpretable principal component and weight function estimates at each level via LVPCA individually for the matrices $\widehat{K}_z$ and $\widehat{K}_w$ obtained in the first stage. To ease notation, in this and following sections, we will use K and ϕ to represent an estimated covariance function and its eigenvector, which can represent either the between-subject quantities $\widehat{K}_z$ and $\widehat{\phi}^z$ or the within-subject $\widehat{K}_w$ and $\widehat{\phi}^w$.

4.2.1. *Methodological motivation*   As previously discussed, many approaches for conducting a multi-variate FPCA have been developed. To motivate the proposed LVPCA, here we discuss one such approach introduced by Rice and Silverman (1991) where the roughness across each variate of the eigenvectors is penalized. Formally, given a tuning parameter β, the first eigenvector is estimated by maximizing $\phi^T K \phi$ such that $\|\phi\|_{12} = 1$ and $\phi^T D \phi \leq \beta$, where $\|\phi\|_{12} = (\phi^T \phi)^{1/2}$ is the L_2 vector norm and D is a roughness matrix penalizing the sum of squared second differences across time. Specially, D is the PM × PM block diagonal matrix with *m*th block $D_m = Q^T Q$, and Q is the $(P-2) \times P$ matrix where $Q_{pq} = 1$ when $q \in \{p, p+2\}$, $Q_{pq} = -2$ when $q = p+1$, and is zero otherwise.

It will be advantageous to consider two additional formulations of this estimator. The first, which was used by Rice and Silverman (1991) and allows for the estimator to be computed from a simple singular value decomposition, can be obtained through Lagrange multipliers by maximizing the equivalent problem $\phi^T(K - \gamma D)\phi$ such that $\|\phi\|_{12} = 1$ for some smoothing parameter $\gamma > 0$. Alternatively, this problem can also be expressed as maximizing $\langle K - \gamma D, \phi\phi^T \rangle_{22}$ such that $\|\phi\|_{12} = 1$, where $\langle A, B \rangle_{22} = \text{trace}(A^T B)$. This last formulation will facilitate the convex relaxation of the problem when localization is introduced, assuring the existence of a solution and enabling efficient computation.

The estimated eigenfunctions previously described are smooth, but not localized, either in time or among variates, in the sense that the estimated eigenfunction at every time point within each variate is nonzero with probability 1. An intuitive approach for obtaining localized estimates of the first eigenfunction is to, in a manner similar to the sparse-group Lasso (Simon *and others*, 2013), use a combination of L_1 Lasso and L_2 group-Lasso penalties to maximize

$$\langle K - \gamma D, \phi\phi^T \rangle_{22} - \alpha \sum_{m=1}^{M} \sqrt{P} \|\phi^{(m)}\|_{12} - \lambda \|\phi\|_{11} \text{ s.t. } \|\phi\|_{12} = 1,$$

where $\|\phi\|_{11} = \sum_{m=1}^{M} \sum_{p=1}^{P} |\phi^{(m)}(t_p)|$ is the L_1 vector norm. The tuning parameters $\lambda > 0$ and $\alpha > 0$ control the degree of within- and between-variate localization, respectively. $\gamma, \lambda,$ and α can be selected either through cross-validation to obtain an accurate estimate or by requiring more sparsity with some sacrifice of the fraction of variance explained (FVE). Details for tuning parameter selection are provided in Section 1.2 of the Supplementary material available at *Biostatistics* online.

4.2.2. *Penalized deflated Fantope estimation*   Unfortunately, the previously considered problem is non-convex, it is not clear if or when a solution exists, and if a solution existed, it would be computationally intractable. A computationally tractable and consistent approach can be formulated through a convex relaxation. Approaches for conducting penalized PCA that consider problems embedded within the convex hull of projection matrices have been explored for sparse PCA of high-dimensional multivariate data (Lei *and others*, 2015) and for localized PCA of univariate functional data (Chen and Lei, 2015). Here, we extend this approach to our setting of localized sparse-variate PCA of multivariate functional data.

Rather than attempting to maximize the objective function over the space of rank-one projection matrices of the form $\phi\phi^T$, we can maximize an analogous objective function over the convex hull of rank-one projection matrices, or over the Fantope $\mathcal{F} = \{H : 0 \preceq H \preceq I, \mathrm{trace}(H) = 1\}$, where $A \preceq B$ means $B - A$ is positive semidefinite for symmetric matrices A and B. Formally, we define our estimate as the first eigenvector of the matrix $\widehat{H} \in \mathcal{F}$ that maximizes

$$\langle K - \gamma D, H \rangle_{22} - \alpha \sum_{m,\ell=1}^{M} P \|H^{(m,\ell)}\|_{22} - \lambda \|H\|_{21},$$

where $H^{(m,\ell)}$ is the (m,ℓ)th $P \times P$ submatrix of H and $\|H\|_{21}$ is the L_1 matrix norm that is the sum of the absolute values of all elements.

This approach produces estimates of the first eigenfunction, but we also desire estimates of higher-order eigenfunctions and require the collection of estimated eigenfunctions to be orthogonal. This can be easily achieved within the Fantope framework via successive Fantope-deflation. The deflated Fantope around a projection matrix Π is defined as $\mathcal{D}_\Pi = \{H : H \in \mathcal{F}, \langle H, \Pi \rangle_{22} = 0\}$. Formally, define $\widehat{\Pi}_0$ as a matrix of zeros and successively estimate $\widehat{\phi}_r$ for each $r = 1, ..., R$ as

$$H_r = \underset{H \in \mathcal{D}_{\widehat{\Pi}_{r-1}}}{\mathrm{argmax}} \{\langle K - \gamma D, H \rangle_{22} - \alpha \sum_{m,\ell=1}^{M} P \|H^{(m,\ell)}\|_{22} - \lambda \|H\|_{21}\}$$

$$\widehat{\phi}_r = \text{ first eigenvector of } H_r$$

$$\widehat{\Pi}_r = \widehat{\Pi}_{r-1} + \widehat{\phi}_r \widehat{\phi}_r^T.$$

(4.3)

Once the eigenvectors are obtained, scores ξ can be obtained through the best linear unbiased predictor (BLUP) and eigenvalues θ through empirical moments of the scores. Details for the estimation of ξ and θ are provided in Section 1.3 of the Supplementary material available at *Biostatistics* online.

4.3. *Optimization using ADMM*

The first step in our procedure (4.3) is a convex optimization problem. However, the deflated Fantope constraint makes it difficult to directly employ block-wise subgradient strategy on the penalty terms. To solve this problem, we use the ADMM algorithm to separate the penalty terms and the deflated Fantope constraint. Define $\mathbb{I}_{\mathcal{D}_{\widehat{\Pi}_{r-1}}} = 0$ if $H \in \mathcal{D}_{\widehat{\Pi}_{r-1}}$ and ∞ otherwise, the augmented Lagrangian with auxiliary parameter $\tau > 0$ is of the form $L_\tau(H, A, C) = \mathbb{I}_{\mathcal{D}_{\widehat{\Pi}_{r-1}}}(H) - \langle K - \gamma D, H \rangle_{22} + \alpha \sum_{m,\ell=1}^{M} P \|A^{(m,\ell)}\|_{22} + \lambda \|A\|_{21} + \frac{\tau}{2}(\|H - A + C\|_{22}^2 - \|C\|_{22}^2)$. Letting $S_b(B)$ be the element-wise soft-thresholding operator such that, for each element $B^{[i,j]}$ of a matrix B, $S_b(B)^{[i,j]} = \mathrm{sign}(B^{[i,j]})(|B^{[i,j]}| - b)_+$, and letting $\mathcal{P}_{\mathcal{D}_\Pi}(B) = \underset{E \in \mathcal{D}_\Pi}{\mathrm{argmin}} \|B - E\|_{22}^2$ be the Frobenius projection operator, a closed form of which is given in Supplemental Material, this can be solved through Algorithm 1.

5. SIMULATION

To better understand the empirical performance of the multilevel LVPCA, we conducted simulations based on the following model:

$$Y_{ij}(t_p) = \sum_{r=1}^{R_1} \xi_{ir}^z \phi_r^z(t_p) + \sum_{r=1}^{R_2} \xi_{ijr}^w \phi_r^w(t_p) + \epsilon_{ij}(t_p),$$

(5.4)

Algorithm 1: Penalized deflated Fantope estimation using ADMM

Initialization $A_{(0)} = 0, C_{(0)} = 0, v = 0, 1, 2, ...$

repeat

$$H_{(v+1)} = \mathcal{P}_{\mathcal{D}_{\widehat{\Pi}_{r-1}}} \left(A_{(v)} - C_{(v)} + \frac{K - \gamma D}{\tau} \right)$$

$$A_{(v+1)}^{(m,\ell)} = \left(1 - \frac{\alpha P/\tau}{\|S_{\lambda/\tau}(H_{(v+1)}^{(m,\ell)} + C_{(v)}^{(m,\ell)})\|_{22}} \right)_+ S_{\lambda/\tau} \left(H_{(v+1)}^{(m,\ell)} + C_{(v)}^{(m,\ell)} \right)$$

$$C_{(v+1)} = C_{(v)} + H_{(v+1)} - A_{(v+1)}$$

until $max \left(\left\| H_{(v+1)} - A_{(v+1)} \right\|_{22}^2, \tau^2 \left\| A_{(v+1)} - A_{(v)} \right\|_{22}^2 \right) \leq \omega$;

return $H_{(v+1)}$

---

where $\xi_{ir}^z \sim N(0, \theta_r^z)$, $\xi_{ijr}^w \sim N(0, \theta_r^w)$, $\text{cov}(\xi_{ijr}^w, \xi_{ikr}^w) = \rho_{jk}\theta_r^w$, $\epsilon_{ij}(t) \sim N(0, \sigma^2)$, and $t_p = (p - 1)/(P - 1)$, $i = 1, ..., 100$, $j = 1, ..., 5$, $p = 1, ..., 100$. $M = 3$ variates. The true eigenvalues are taken as $\theta_r^z = \theta_r^w = 0.5^{r-1}, r = 1, 2, 3$, the true correlation coefficient as $\rho_{jk} = 0.5$ when $j = k \pm 1$, $\rho_{jk} = 0.3$ when $j = k \pm 2$, and is zero otherwise, and the noise as $\sigma^2 = 1$. The true eigenfunctions are displayed as black lines in Figure 2. To evaluate the relative contributions of the localization and sparsity penalties, and of the estimation of within-subject correlation, we consider eight estimation procedures denoted as: $(\hat{\alpha}, \hat{\lambda}, \hat{\rho}), (\hat{\alpha}, 0, \hat{\rho}), (0, \hat{\lambda}, \hat{\rho}), (0, 0, \hat{\rho}), (\hat{\alpha}, \hat{\lambda}, 0), (\hat{\alpha}, 0, 0), (0, \hat{\lambda}, 0), (0, 0, 0)$. The first procedure $(\hat{\alpha}, \hat{\lambda}, \hat{\rho})$ corresponds to the proposed LVPCA with α, λ, and γ selected by 5-fold cross-validation, and ρ estimated as described in Appendix A.3 of the Supplementary material available at *Biostatistics* online. Other procedures restrict one or more of $\hat{\alpha}, \hat{\lambda}$, or $\hat{\rho}$ to 0.

Figure 2 displays estimated eigenfunctions ϕ_r^z and $\phi_r^w, r = 1, 2, 3$, from one simulated data set. The eight rows correspond to the eight methods. The solid black lines are the true eigenfunctions, green lines indicate estimated zero elements and red lines indicate estimated nonzero elements. Visually, in the top row of Figure 2, it can be seen that the proposed LVPCA, which includes within-variate localization, between-variate sparseness penalties and accounting for within-subject correlation between electrode-specific deviations, leads to favorable recovery of eigenfunctions. Removing either penalty appears to potentially increase bias and select more nonzero elements of ϕ_r^z than the truth. Failing to adjust for within-subject correlation between electrode-specific deviations can negatively affect the accuracy of the shape of $\hat{\phi}_3^z$, since the between-subject variation is contaminated by the within-subject variation, specifically $\hat{\phi}_3^z$ is contaminated by $\hat{\phi}_1^w$. This trend is further quantified in Table 2, where we report the median of the errors $\|\phi - \hat{\phi}\|_2$, as well as in Table 3, where we report the median specificity and sensitivity (proportion nonzero/zero elements correctly estimated as nonzero/zero). The proposed LVPCA outperforms the other methods in eigenvector estimation particularly for the higher-level of the hierarchy, and also has the highest specificity among all the methods, and a reasonable level of sensitivity. This result demonstrates the advantage of the proposed LVPCA, which combines localization and between-variate sparsity penalties, in terms of both estimation and variable selection.

In terms of estimation of subject- and electrode-level eigenvalues, the four methods that adjust for within-subject correlation between electrode-specific deviations can recover eigenvalues with relatively little bias; median bias for these methods ranged from -0.006 to 0.022. On the contrary, the four methods without adjusting for within-subject correlation over-estimate θ_3^z, with median bias ranging from 0.082
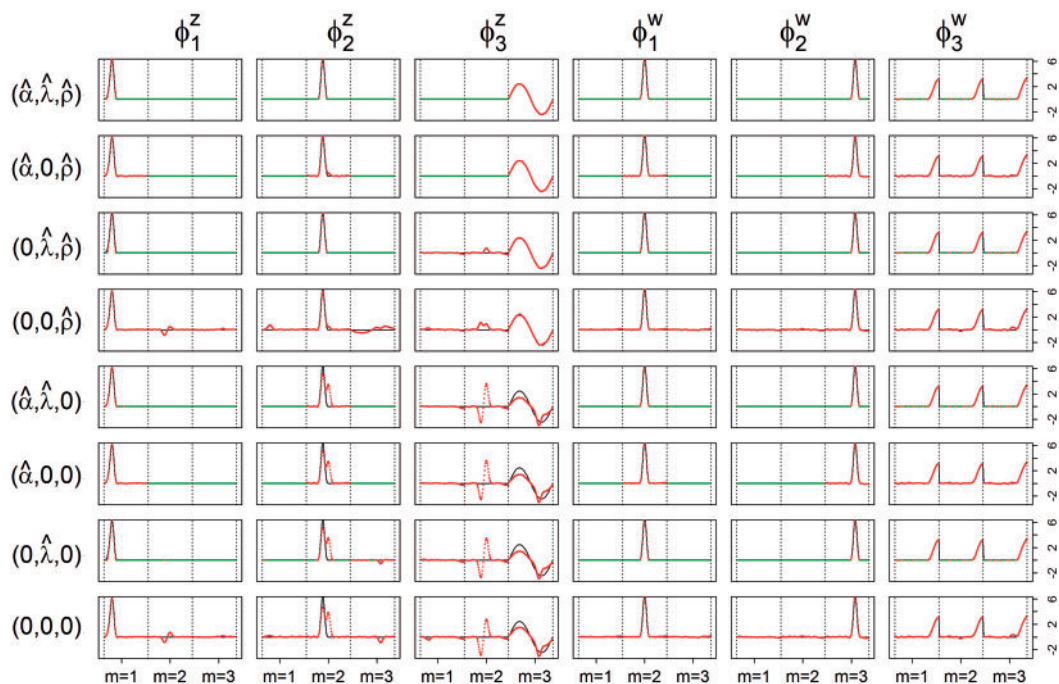
Fig. 2. True (black solid) and estimated (green and red dot) eigenfunctions from one simulated data set by the described eight estimation procedures. Solid black lines are the true eigenfunctions, green lines indicate estimated zero elements, and red lines indicate estimated nonzero elements.

Table 1. *True eigenfunctions in the simulation setting presented in Section 5. The function $B_b(t)$ is the bth cubic B-spline basis on $[0, 1]$, with 16 equally spaced interior knots, and $(t)_+ = t$ when $t \geq 0$ and is zero otherwise.*

	$m = 1$	$m = 2$	$m = 3$
$\phi_1^z(t)$	$B_4(t)$	0	0
$\phi_2^z(t)$	0	$B_7(t)$	0
$\phi_3^z(t)$	0	0	$\sqrt{2}\sin(2\pi t)$
$\phi_1^w(t)$	0	$B_9(t)$	0
$\phi_2^w(t)$	0	0	$B_{12}(t)$
$\phi_3^w(t)$	$\sqrt{2}\cos\left[\pi(t - \frac{3}{4})\right](t - \frac{3}{4})_+$	$\sqrt{2}\cos\left[\pi(t - \frac{3}{4})\right](t - \frac{3}{4})_+$	$\sqrt{2}\cos\left[\pi(t - \frac{3}{4})\right](t - \frac{3}{4})_+$

to 0.088, and highly underestimate θ_1^w, θ_2^w, and θ_3^w, with median bias ranging from -0.290 to -0.072. This can be attributed to part of the within-subject variation is mistakenly counted as between-subject variation. Additional details including empirical performance in estimating principal component scores, noise level and within-subject correlation, boxplots of estimated eigenvalues, as well as simulation results for additional settings are provided in Section 3 of the Supplementary material available at *Biostatistics* online. The primary factor affecting run time is $M \times P$, with N and J having little relative effect. In our simulations, the mean run time for the proposed procedure including automated tuning parameter

Table 2. *Median errors* $\|\phi - \widehat{\phi}\|_2$ *for* $\phi_r^z, \phi_r^w, r = 1, 2, 3$ *(with median absolute deviations in parenthesis) over 200 simulation runs.*

	ϕ_1^z	ϕ_2^z	ϕ_3^z	ϕ_1^w	ϕ_2^w	ϕ_3^w
$(\hat{\alpha}, \hat{\lambda}, \hat{\rho})$	0.49 (0.15)	0.91 (0.41)	2.18 (1.15)	0.34 (0.04)	0.41 (0.04)	0.66 (0.10)
$(\hat{\alpha}, 0, \hat{\rho})$	0.60 (0.15)	1.89 (0.68)	2.54 (1.50)	0.66 (0.08)	1.11 (0.11)	0.91 (0.10)
$(0, \hat{\lambda}, \hat{\rho})$	1.25 (0.31)	0.96 (0.44)	3.49 (1.13)	0.41 (0.09)	0.41 (0.05)	0.60 (0.09)
$(0, 0, \hat{\rho})$	2.67 (0.78)	3.89 (1.00)	4.46 (1.23)	1.43 (0.43)	2.14 (0.58)	1.57 (0.44)
$(\hat{\alpha}, \hat{\lambda}, 0)$	0.48 (0.14)	1.09 (0.62)	23.14 (1.56)	0.33 (0.03)	0.42 (0.05)	0.66 (0.10)
$(\hat{\alpha}, 0, 0)$	0.61 (0.15)	3.46 (1.73)	11.71 (5.99)	0.66 (0.08)	1.11 (0.11)	0.90 (0.09)
$(0, \hat{\lambda}, 0)$	1.30 (0.37)	1.19 (0.72)	15.15 (8.45)	0.42 (0.09)	0.41 (0.05)	0.60 (0.09)
$(0, 0, 0)$	3.02 (0.88)	5.52 (1.71)	12.73 (4.39)	1.43 (0.43)	2.14 (0.58)	1.57 (0.44)

Table 3. *Median of specificity (proportion of zero elements correctly estimated as zero) and sensitivity (proportion of nonzero elements estimated as nonzero) for* $\phi_r^z, \phi_r^w, r = 1, 2, 3$*, over 200 simulation runs.*

	Specificity						Sensitivity					
	ϕ_1^z	ϕ_2^z	ϕ_3^z	ϕ_1^w	ϕ_2^w	ϕ_3^w	ϕ_1^z	ϕ_2^z	ϕ_3^z	ϕ_1^w	ϕ_2^w	ϕ_3^w
$(\hat{\alpha}, \hat{\lambda}, \hat{\rho})$	0.99	0.99	1.00	0.99	1.00	0.75	0.87	0.83	1.00	0.92	0.92	0.85
$(\hat{\alpha}, 0, \hat{\rho})$	0.75	0.73	1.00	0.73	0.73	0.01	1.00	1.00	1.00	1.00	1.00	1.00
$(0, \hat{\lambda}, \hat{\rho})$	0.97	1.00	0.03	1.00	1.00	0.75	0.71	0.83	1.00	0.76	0.80	0.85
$(0, 0, \hat{\rho})$	0.02	0.01	0.02	0.02	0.02	0.01	1.00	1.00	1.00	1.00	1.00	1.00
$(\hat{\alpha}, \hat{\lambda}, 0)$	0.99	0.98	0.86	1.00	1.00	0.74	0.87	0.88	0.56	0.88	0.92	0.85
$(\hat{\alpha}, 0, 0)$	0.75	0.73	0.50	0.73	0.73	0.01	1.00	1.00	1.00	1.00	1.00	1.00
$(0, \hat{\lambda}, 0)$	0.97	0.99	0.82	1.00	1.00	0.75	0.71	0.79	0.91	0.76	0.80	0.85
$(0, 0, 0)$	0.02	0.01	0.02	0.02	0.02	0.01	1.00	1.00	1.00	1.00	1.00	1.00

selection with $P = 100$ and $M = 3$ using R Version 3.4 and Windows 10 on a desktop computer with a 3.6 GHz Intel Core i7 processor and 8 GB RAM is 3 min, while the data analysis of the motivating study in Section 6 where $M = 4$ and $P = 143$ took approximately 25 min.

6. APPLICATION TO THE BADA STUDY

We applied the proposed methodology to analyze brain reactivity while ruminating on a negative thought from the participants in the BADA study described in Section 2. These data are available from the corresponding author upon request. EEG data considered for each of the $i = 1, \ldots, N = 106$ study participants are of the form $Y_{ij}^{(m)}(t_p)$ for $m = 1, \ldots, 4$ frequency bands (theta, alpha, beta, and gamma), at $j = 1, \ldots, J = 14$ electrodes (locations displayed in Figure 4(A)). Data were pre-centered around each electrode at each time point to remove fixed effects. In Section 6.1, LVPCA was conducted on both the between-subject and within-subject levels to elucidate variability in neurophysiological activity in patients while ruminating on negative thoughts. Then, in Section 6.2, regression analyses were conducted using the scores obtained from the LVPCA to quantify associations between brain activity and clinical dissociation, and for assessing moderation of this relationship by a history of trauma.
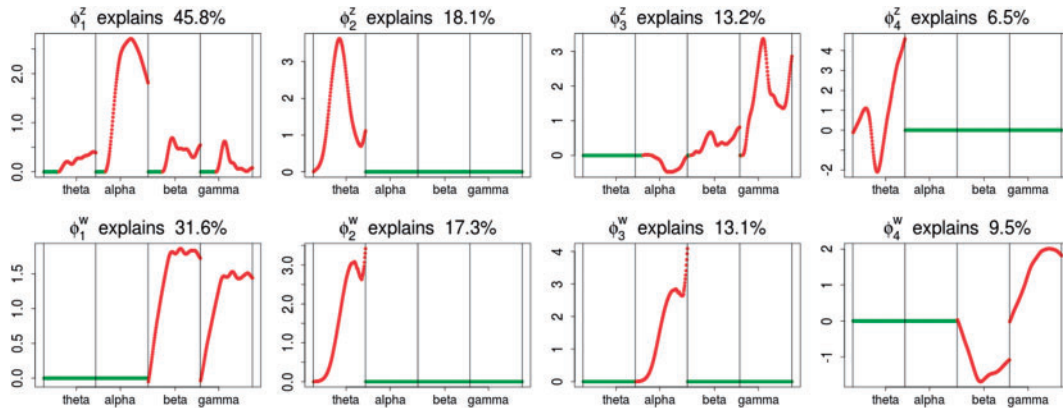
Fig. 3. Estimated subject-level (top row) and electrode-level (bottom row) eigenfunctions for the BADA Study. Green lines indicate estimated zero elements and red lines indicate estimated nonzero elements.

6.1. *LVPCA*

Four principal components at both within- and between-subject levels were selected to account for 75% of total variation (Figure 3). The top four subject-level principal components explain 83.6% of the total between-subject variation. The first estimated subject-level eigenfunction $\phi_1^z(t)$ explains 45.8% of the variation. It is localized within each variate, being zero for each frequency band in the first 3 s of the trial, with an emphasis on alpha power. The second estimated subject-level eigenfunction $\phi_2^z(t)$, accounting for 18.1% of the variation, is sparse among bands and is a measure of total theta power, with greatest emphasis given to power in the middle of the trial. The third component $\phi_3^z(t)$ is a contrast between beta and gamma power compared to alpha power. The fourth eigenfunction $\phi_4^z(t)$ is a contrast in theta power at the beginning and end of the trial.

Subject-level eigenfunctions represent the major directions of subject-specific deviation from the overall mean power function. It is not entirely unexpected that they are largely driven by theta and alpha power. Participants were observed while ruminating on a negative memory. Theta power has been linked to memory (Knyazev, 2007), and alpha power has been associated with a lack of emotional regulatory control (Klimesch, 2012), two processes underlying rumination.

The electrode-level components represent ways individual participants vary from population mean and subject-specific whole-brain responses to rumination at specific electrodes. Estimated mean topologies of responses to the rumination instruction across all frequency bands $\widehat{\eta}_j(t)$ are displayed in Section 2.4.2 of the Supplementary material available at *Biostatistics* online. The top four estimated electrode-level principal components explained 71.5% of the total within-subject variation. All four estimated components are sparse among frequency bands. The first estimated electrode-level eigenfunction $\phi_1^w(t)$ is a positive function of beta and gamma power, or of high-frequency power. Rapidly increasing sustained high-frequency activity could represent effortful cognition associated with trying to ruminate or to regulate emotional reactions. The estimated second and third electrode-level eigenfunctions $\phi_2^w(t)$ and $\phi_3^w(t)$ are positive functions of theta and alpha power, respectively. The fourth estimated electrode-level eigenfunction $\phi_4^w(t)$ is a positive function of gamma and a negative function of beta power, which could reflect emotional engagement or feature binding.

6.2. *Association between principal component scores and dissociation*

Since the principal component scores are correlated, we fit individual regression models for each principal component so that results can be interpreted marginally. In total, there are 60 principal component scores

Table 4. *Coefficients, standard errors, and adjusted p-values from univariate models with significant interaction effects and borderline significant trend of interaction effects.*

	Score		Trauma		Score $\times$ Trauma	
	β_1 (SE)	p-value	β_2 (SE)	p-value	β_3 (SE)	p-value
ξ_2^z	0.65 (0.56)	0.999	1.66 (0.25)	<0.001	−2.67 (0.89)	0.027
$\xi_{1,\,O1}^w$	1.01 (0.40)	0.098	1.62 (0.25)	<0.001	−1.73 (0.59)	0.036
$\xi_{3,\,FC6}^w$	−0.43 (0.39)	0.27	1.68 (0.26)	<0.001	2.10 (0.80)	0.082
$\xi_{3,\,F8}^w$	−0.31 (0.40)	0.45	1.74 (0.26)	<0.001	2.21 (0.84)	0.082

per subject: the four subject-specific scores ξ_{ir}^z together with the $14 \times 4 = 56$ subject-electrode-specific scores ξ_{ijr}^w, $r = 1, \ldots, 4$, $j = 1, \ldots, 14$. All reported p-values are adjusted to control the false discovery rate (FDR) at 0.05 with the adaptive group Benjamin and Hochberg procedure (details in Section 2.2 of the Supplementary material available at *Biostatistics* online).

Let Y_i be the square root transformed DES score, V_i be an indicator variable for a history of trauma, and X_i be a principal component score for subject i. We fit the linear regression model $\mathrm{E}\,(Y_i) = \beta_0 + \beta_1 X_i + \beta_2 V_i + \beta_3 X_i V_i$ through least squares individually for each of 60 principal component scores. The coefficient β_1, which quantifies the association between principal component score and square root transformed DES score among participants without a history of trauma, was not statistically significant for any of the principal component scores. The coefficient β_2, which is the main effect of trauma, was statistically significant and positive for all principal component scores adjusting for multiple comparisons. This is not unexpected, since dissociation is more common among those with a history of trauma. There were two principal component scores with significant interactions after adjusting for multiple comparisons, indicating that the relationship between brain activity and dissociation is moderated by trauma: one subject-level and one electrode-level. Table 4 displays estimates from the two models with significant interactions and two models with borderline significant trend of interaction effects. Estimates from all 60 models are provided in Section 2.3 of the Supplementary material available at *Biostatistics* online, as well as scatter plots of principal component scores vs. transformed DES for the models presented in Table 4.

Among the four subject-level principal component scores, the sole model with a significant interaction was ξ_2^z. For this component, the adjusted p-value of β_1 of 0.999 suggests no association between the score and dissociation in people without a history of trauma, while $\widehat{\beta_1 + \beta_3} = -2.02$ with adjusted p-value 0.028 indicates a negative association in people with a history of trauma. More specifically, recalling that the estimated second subject-level component is a measures of whole-brain theta power, if a person has a history of trauma, the higher his/her theta power, the lower their expected dissociation level. Theta power is associated with memory and emotional control and has been shown to be elevated in participants with a history of PTSD (Bangel *and others*, 2017). This result may suggest that during instructed rumination, if a person has a history of trauma, not engaging memory related circuitry, perhaps failing to reinvoke trauma recollections, even when a person wants to, may involve dissociation. In the absence of a trauma history, dissociation during rumination may be due to processes other than intensive memory recall, and thus theta power is not so strongly related to dissociation. However, it should be noted that whole-brain theta variability may also represent noise sources (Kappel *and others*, 2017; Zeng *and others*, 2013; Jansen *and others*, 2012) from outside the brain (e.g., movement). Further study is needed to confirm if the moderating effect of trauma on the relationship between dissociation and this score is due to neural processes, or the result of a confounding artifact.

Figure 4 displays the adjusted p-values of the interaction effects for the 1st and 3rd electrode-level components at the 14 locations of the brain. The 2nd and 4th components have no effect near significant,

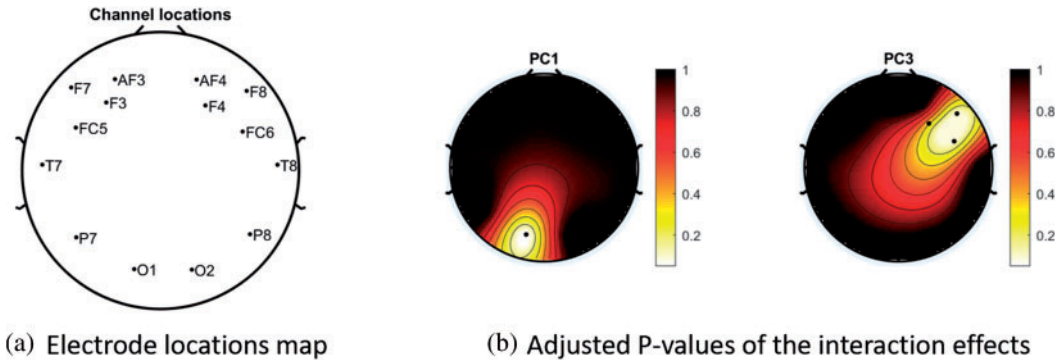(a) Electrode locations map   (b) Adjusted P-values of the interaction effects

Fig. 4. (A) Locations of the 14 electrodes on the brain. (B) Adjusted p-values for the interaction effect of electrode-level PC 1 and PC 3 scores across 14 electrodes displayed on their corresponding locations. White color indicates locations with p-value < 0.05.

therefore they are not shown. The model with the 1st principal component score ξ_1^w at electrode O1 has a significant interaction effect with a history of trauma on dissociation. Specifically, among patients without a history of trauma, $\hat{\beta}_1 = 1.01$ suggests elevated beta and gamma power within the occipital cortex relative to the rest of the brain has a trend of being associated with increased dissociation, though the adjusted p-value is not significant (adjusted p-value $= 0.098$). However this association is significantly different (adjusted p-value $= 0.036$) among patients with a history of trauma, where elevated beta and gamma power within the occipital cortex relative to the rest of the brain has a negative effect on dissociation with $\widehat{\beta_1 + \beta_3} = -0.72$. The reason for an occipital distribution of beta and gamma power is not clear but may suggest that failure of cognitive concentration and regulation of emotional reactions may involve dissociation among individuals with a history of trauma, while this association may have an opposite effect in the absence of trauma history. Other scores that have different directions of associations include ξ_3^w at electrode FC6 and F8. Although such differences are not significant after adjusting for multiple testing (adjusted p-value $= 0.082$), it is worth noticing that elevated alpha power within the right frontal cortex relative to the rest of the brain has a trend of positive effect on the increased dissociation in patients with a history of trauma ($\widehat{\beta_1 + \beta_3} = 1.90$), which did not appear among patients without a history of trauma ($\hat{\beta}_1 = -0.31$, adjusted p-value $= 0.45$).

7. DISCUSSION

This article introduces a novel approach to conducting interpretable principal component analysis on multilevel multivariate functional data. The proposed localized sparse-variate FPCA (LVPCA) is combined with a multilevel covariance decomposition to provide subject-level and replicate-within-subject-level components that can be both sparse among variates as well as localized in time. The method was motivated by a study to uncover subject- and electrode-level brain activity that elucidates neurophysiological mechanisms connected to the phenomena of trauma patients shutting down when presented with emotional information.

The proposed method can be easily reduced to useful special cases and generalized to handle more complicated data structures. By restricting $\alpha = 0$ and/or $\lambda = 0$, the method reduces to localized FPCA, sparse-variate FPCA or FPCA without any localization. When $J = 1$ or $m = 1$, the method reduces to FPCA on single level or univariate functional data. The proposed method together with all the special cases are implemented into an R package "LVPCA" to facilitate future research. The method can be extended by incorporating other penalty terms to take into account special structures induced by biological information (Beer *and others*, 2019). Further, the method can be generalized from two-way to multiway, nested or

crossed study designs, as introduced in Shou *and others* (2015). If the design is unbalanced with different number of repeated measures per subject, we can modify the covariance estimators by including only available $(Y_{ij} - Y_{nk})(Y_{ij} - Y_{nk})^T$ as each of the cross-products independently contributes a same estimator when estimating the between- and within-subject covariance.

Finally, in our motivating example, curves were observed over a common dense grid of P time points. When curves are observed over different time grids, presmoothing can be used to obtain data over a common grid of time points (Ramsay and Silverman, 2005). If each subject is only observed over a sparse collection of random time points, a direct smoothed covariance estimator for sparse functional data (Yao *and others*, 2005) could be used in lieu of the sample covariance and smoothing penalization component of the proposed procedure.

8. SOFTWARE

Software in the form of R code, together with a sample input data set, is available at
https://github.com/juz30/MLVPCA.

SUPPLEMENTARY MATERIAL

Supplementary material is available online at http://biostatistics.oxfordjournals.org.

ACKNOWLEDGMENTS

FUNDING

REFERENCES

BANGEL, K. A., VAN BUSCHBACH, S., SMIT, D. J. A., MAZAHERI, A. AND OLFF, M. (2017). Aberrant brain response after auditory deviance in PTSD compared to trauma controls: an eeg study. *Scientific Reports* **7**, 16596.

BEER, J. C., AIZENSTEIN, H. J., ANDERSON, S. J. AND KRAFTY, R. T. (2019). Incorporating prior information with fused sparse group lasso: application to prediction of clinical measures from neuroimages. *Biometrics* **75**, 1299–1309.

BERNSTEIN, E. M. AND PUTNAM, F. W. (1986). Development, reliability, and validity of a dissociation scale. *Journal of Nervous and Mental Disease* **174**, 727–735.

BOYD, S., PARIKH, N., CHU, E., PELEATO, AND B. ECKSTEIN, J. (2011). Distributed optimization and statistical learning via the alternating direction method of multipliers. *Foundations and Trends® in Machine learning* **3**, 1–122.

CHEN, K. AND LEI, J. (2015). Localized functional principal component analysis. *Journal of the American Statistical Association* **110**, 1266–1275.

CHEN, K. AND MÜLLER, H.-G. (2012). Modeling repeated longitudinal observations. *Journal of the American Statistical Association* **107**, 1599–1609.

CHIOU, J.-M., CHEN, Y.-T. AND YANG, Y.-F. (2014). Multivariate functional principal component analysis: a normalization approach. *Statistica Sinica* **24**, 1571–1596.

CRAINICEANU, C. M., STAICU, A.-M. AND DI, C.-Z. (2009). Generalized multilevel functional regression. *Journal of the American Statistical Association* **104**, 1550–1561.

Davidson, R. J., Ekman, P., Saron, C. D., Senulis, J. A. and Friesen, W. V. (1990). Approach-withdrawal and cerebral asymmetry: emotional expression and brain physiology: I. *Journal of Personality and Social Psychology* **58**, 330.

Di, C.-Z., Crainiceanu, C. M., Caffo, B. S. and Punjabi, N. M. (2009). Multilevel functional principal component analysis. *The Annals of Applied Statistics* **3**, 458.

Goldsmith, J., Zipunnikov, V. and Schrack, J. (2015). Generalized multilevel function-on-scalar regression and principal component analysis. *Biometrics* **71**, 344–353.

Greven, S., Crainiceanu, C., Caffo, B. and Reich, D. (2010). Longitudinal functional principal component analysis. *Electronic Journal of Statistics* **4**, 1022–1054.

Happ, C. and Greven, S. (2018). Multivariate functional principal component analysis for data observed on different (dimensional) domains. *Journal of the American Statistical Association* **113**, 649–659.

Hasenstab, K., Scheffler, A., Telesca, D., Sugar, C. A., Jeste, S., Distefano, C. and Şentürk, D. (2017). A multi-dimensional functional principal components analysis of eeg data. *Biometrics* **73**, 999–1009.

James, G. M., Wang, J. and Zhu, J. (2009). Functional linear regression that's interpretable. *The Annals of Statistics* **37**, 2083–2108.

Jansen, M., White, T. P., Mullinger, K. J., Liddle, E. B., Gowland, P. A., Francis, S. T., Bowtell, R. and Liddle, P. F. (2012). Motion-related artefacts in EEG predict neuronally plausible patterns of activation in fMRI data. *Neuroimage* **59**, 261–270.

Kappel, S. L., Looney, D., Mandic, D. P. and Kidmose, P. (2017). Physiological artifacts in scalp EEG and ear-EEG. *Biomedical Engineering Online* **16**, 103.

Klimesch, W. (2012). Alpha-band oscillations, attention, and controlled access to stored information. *Trends in Cognitive Sciences* **16**, 606–617.

Knyazev, G. G. (2007). Motivation, emotion, and their inhibitory control mirrored in brain oscillations. *Neuroscience & Biobehavioral Reviews* **31**, 377–395.

Lei, J. and Vu, V. Q. (2015). Sparsistency and agnostic inference in sparse PCA. *The Annals of Statistics* **43**, 299–322.

Lin, Z., Wang, L.g and Cao, J. (2016). Interpretable functional principal component analysis. *Biometrics* **72**, 846–854.

Miniati, M., Rucci, P., Benvenuti, A., Frank, E., Buttenfield, J., Giorgi, G. and Cassano, G. B. (2010). Clinical characteristics and treatment outcome of depression in patients with and without a history of emotional and physical abuse. *Journal of Psychiatric Research* **44**, 302–309.

Neuper, C., Scherer, R., Wriessnegger, S. and Pfurtscheller, G. (2009). Motor imagery and action observation: modulation of sensorimotor brain rhythms during mental control of a brain–computer interface. *Clinical Neurophysiology* **120**, 239–247.

Ramsay, J. O. and Silverman, B. W. (2005). *Functional Data Analysis*, 2nd edition. Springer Series in Statistics. New York: Springer.

Rice, J. A. and Silverman, B. W. (1991). Estimating the mean and covariance structure nonparametrically when the data are curves. *Journal of the Royal Statistical Society: Series B (Methodological)* **53**, 233–243.

Scheffler, A., Telesca, D., Li, Q., Sugar, C. A., Distefano, C., Jeste, S. and Şentürk, D. (2019). Hybrid principal components analysis for region-referenced longitudinal functional EEG data. *Biostatistics*.

Shou, H., Zipunnikov, V., Crainiceanu, C. M. and Greven, S. (2015). Structured functional principal component analysis. *Biometrics* **71**, 247–257.

Simon, N., Friedman, J., Hastie, T. and Tibshirani, R. (2013). A sparse-group lasso. *Journal of Computational and Graphical Statistics* **22**, 231–245.

STAICU, A.-M., CRAINICEANU, C. M. AND CARROLL, R. J. (2010). Fast methods for spatially correlated multilevel functional data. *Biostatistics* **11**, 177–194.

TALLON-BAUDRY, C.E AND BERTRAND, O. (1999). Oscillatory gamma activity in humans and its role in object representation. *Trends in Cognitive Sciences* **3**, 151–162.

VU, V. Q., CHO, J., LEI, J. AND ROHE, K. (2013). Fantope projection and selection: a near-optimal convex relaxation of sparse PCA. In: C. J. C. Burges and L. Bottou and M. Welling and Z. Ghahramani and K. Q. Weinberger (eds) *Advances in Neural Information Processing Systems*. Curran Associates, Inc. pp. 2670–2678.

YAO, F., MÜLLER, H.-G. AND WANG, J.-L. (2005). Functional data analysis for sparse longitudinal data. *Journal of the American Statistical Association* **100**, 577–590.

ZENG, H., SONG, A., YAN, R. AND QIN, H. (2013). EOG artifact correction from eeg recording using stationary subspace analysis and empirical mode decomposition. *Sensors* **13**, 14839–14859.

ZHAO, Y., OGDEN, R. T. AND REISS, P. T. (2012). Wavelet-based lasso in functional linear regression. *Journal of Computational and Graphical Statistics* **21**, 600–617.

ZHOU, J., WANG, N.-Y. AND WANG, N. (2013). Functional linear model with zero-value coefficient function at sub-regions. *Statistica Sinica* **23**, 25.

ZIPUNNIKOV, V., CAFFO, B., YOUSEM, D. M., DAVATZIKOS, C., SCHWARTZ, B. S. AND CRAINICEANU, C. (2011). Multilevel functional principal component analysis for high-dimensional data. *Journal of Computational and Graphical Statistics* **20**, 852–873.